Modelling of PFC melt dynamics

S. Ratynskaia

[a] *Space and Plasma Physics - KTH Royal Institute of Technology, SE-10044, Stockholm, Sweden*

L. Vignitchouk, P. Tolias, F. Lucco Castello

Space and Plasma Physics - KTH Royal Institute of Technology, SE-10044, Stockholm, Sweden

R. A. Pitts

ITER Organization, Route de Vinon-sur-Verdon, F-13067, St. Paul Lez Durance, France

K. Krieger

Max-Planck-Institut fur Plasmaphysik, 85748 Garching b. Munchen, Germany

Outline

- Motivation
- General characteristics of melt events in fusion devices
- How to incorporate plasma effects
- Approaches for the modelling of large and small scale melt dynamics
- Physics model & boundary conditions of the MEMOS-U code
- Keys aspects of melt dynamics in fusion devices (examples)
- Limitation of escaping thermionic emission
- Summary & outlook

Motivation

- The provision of plasma-facing components [PFCs] with sufficient lifetime is one of the major technological obstacles in the development of fusion reactors.

- In ITER, PFC integrity is mostly threatened by fast transient power loading due to magnetohydrodynamic [MHD] instabilities such as edge-localized modes [ELMs], vertical displacement events [VDEs] or major disruptions [MDs].

- In DEMO, the PFC heat load capability will be surpassed during regular plasma ramp-up/-down and undesired events such as the H-L transition, VDEs or MDs.

- Metallic melt motion under plasma-induced forces causes large-scale wall deformations and, in unstable cases, can produce droplets that are released into the vessel.
  - The deformations compromise the PFC power-handling capabilities and shorten their lifetime
  - Ejected droplets are the main source of solid dust whose amount is limited by safety regulations.

- Understanding the physics and consequences of melt motion is of profound importance to the development of fusion devices with metal PFCs.

General characteristics of melt events in fusion devices

J. Coenen *et al* 2015 *NF* **55**

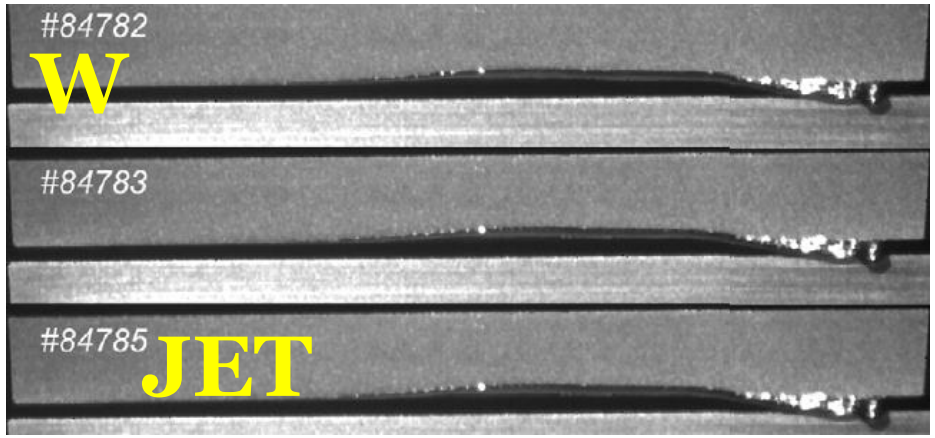

K. Krieger *et al* 2018 *NF* **58**

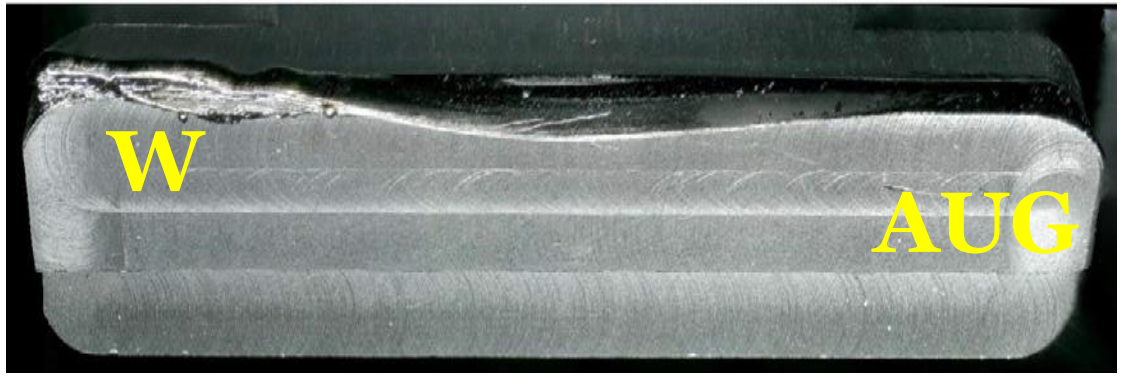

I. Jepu *et al* 2019 *NF* **59**

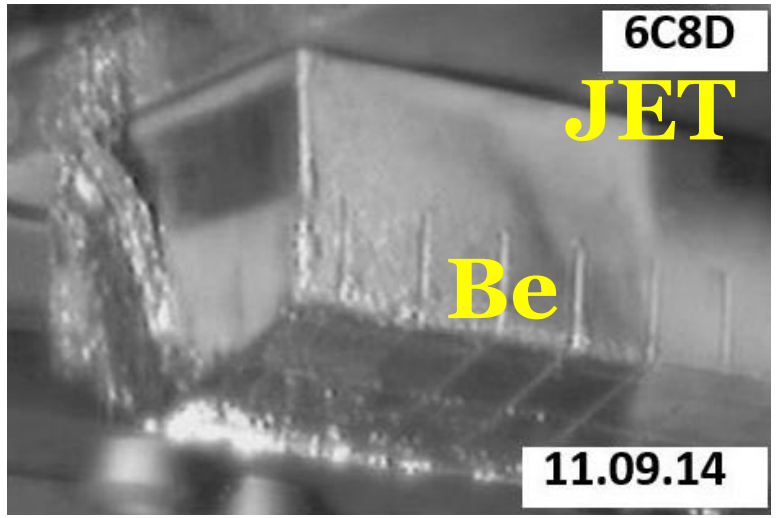

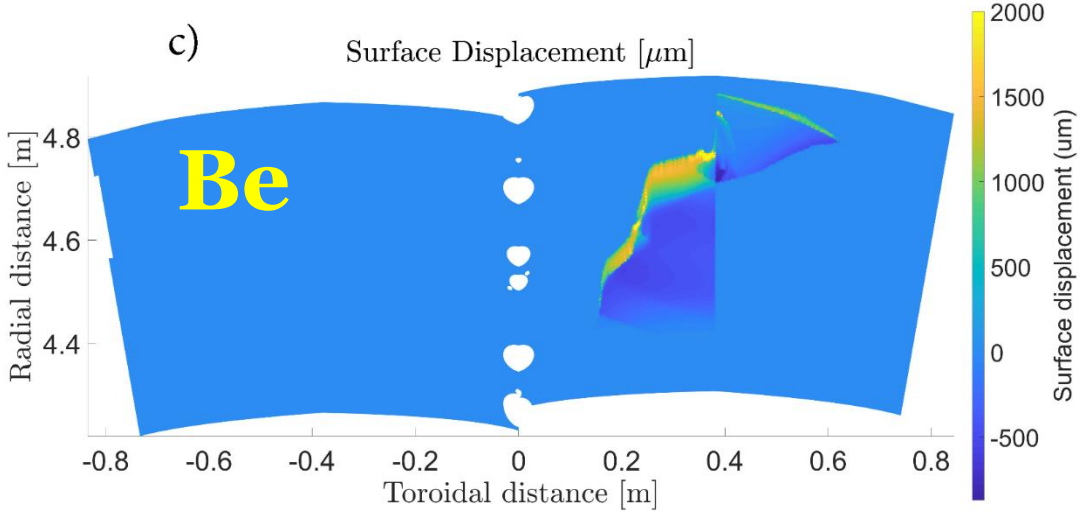

MEMOS-U prediction for surface normal deformation, after 200 ms exposure to an unmitigated VDE on **ITER FWP8**
[J. Coburn, E. Thorén et al. *Phys. Scr.* **T171** 2019].

- Limited wetted area → newly formed liquid pools surrounded by cold(er) solid surfaces.
- Large displacements
- Hot melt flows onto the colder adjacent surface → prompt re-solidification

Dynamics of liquid melts

Governed by the set of incompressible resistive thermoelectric magnetohydrodynamic (TEMHD) equations together with the convection-diffusion equation for the temperature Shercliff J. A. 1979 *J. Fluid Mech.* **91** 231

$$\nabla \cdot \boldsymbol{v} = 0,$$

$$\rho_m \left[\frac{\partial \boldsymbol{v}}{\partial t} + (\boldsymbol{v} \cdot \nabla)\, \boldsymbol{v} \right] = -\nabla p + \mu \nabla^2 \boldsymbol{v} + \boldsymbol{J} \times \boldsymbol{B},$$

$$\rho_m c_p \left[\frac{\partial T}{\partial t} + \boldsymbol{v} \cdot \nabla T \right] = \nabla \cdot (k \nabla T - S T \boldsymbol{J}) + \boldsymbol{J} \cdot \boldsymbol{E},$$

$$\nabla \times \boldsymbol{E} = -\frac{\partial \boldsymbol{B}}{\partial t},$$

$$\nabla \times \boldsymbol{B} = \mu_0 \boldsymbol{J},$$

$$\boldsymbol{J} = \sigma_e \left(\boldsymbol{E} + \boldsymbol{v} \times \boldsymbol{B} - S \nabla T \right),$$

(v, T) fluid velocity, temperature,
$(p, \boldsymbol{J})$ fluid pressure, current density,
$(\boldsymbol{B}, \boldsymbol{E})$ magnetic flux density, electric field strength,
(ρ_m, c_p) mass density, heat capacity
(k, S) thermal conductivity, thermoelectric power,
(μ, γ) dynamic viscosity, surface tension
(σ_e, μ_0) electrical conductivity, vacuum permeability

PFC melting: Multiphase flow with envolving interfaces

Free-surface MHD flows with phase transitions

- fluid dynamics
- heat diffusion
- melting and re-solidification
- current distribution into the PFC bulk

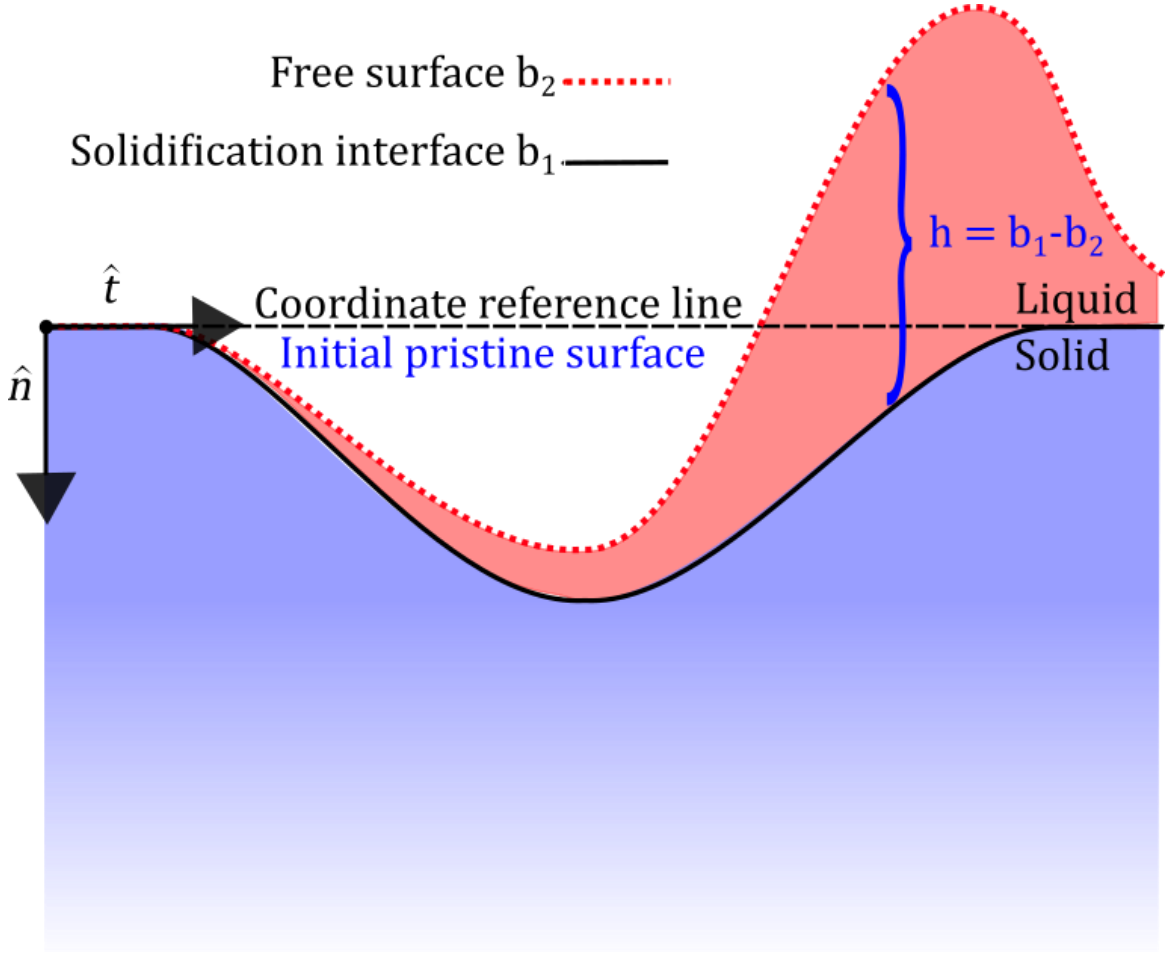

Multi-scale nature of the phenomena

- macroscopic motion along the PFC -- up to fraction of a meter
- the melt depth -- 100's of μm
- nonlinear free -surface instabilities on much smaller scales

Brute-force computations of the fully self-consistent model on the relevant scales are computationally prohibitive

‘ Zoom-in ’ on small domains to study stability and splashing

Seek simplifications if large-scale motion is of interest

How to incorporate plasma effects

- Commercial software allows treating plasma as a real fluid

However in fusion applications, this poses

- numerical problems due to the large disparity between the plasma and metallic densities (factor 10^{10})
- but also a conceptual issue: *near-surface dynamics of magnetized plasmas is driven by electromagnetic processes of kinetic origin*

- In PFC melting events, the retroaction of the melt on the plasma is of little practical interest.
- Plasma modelling can be omitted as long as the proper (kin., dyn., therm.,EM) boundary conditions are *imposed on the free surface.*

- Enforcing *general* interface conditions that correspond to *realistic* situations and geometries remains a challenge that lies way beyond the customization capabilities of commercial software.

Ion backscattering yields plots
from [W. Eckstein (2009) IPP report 17/12].

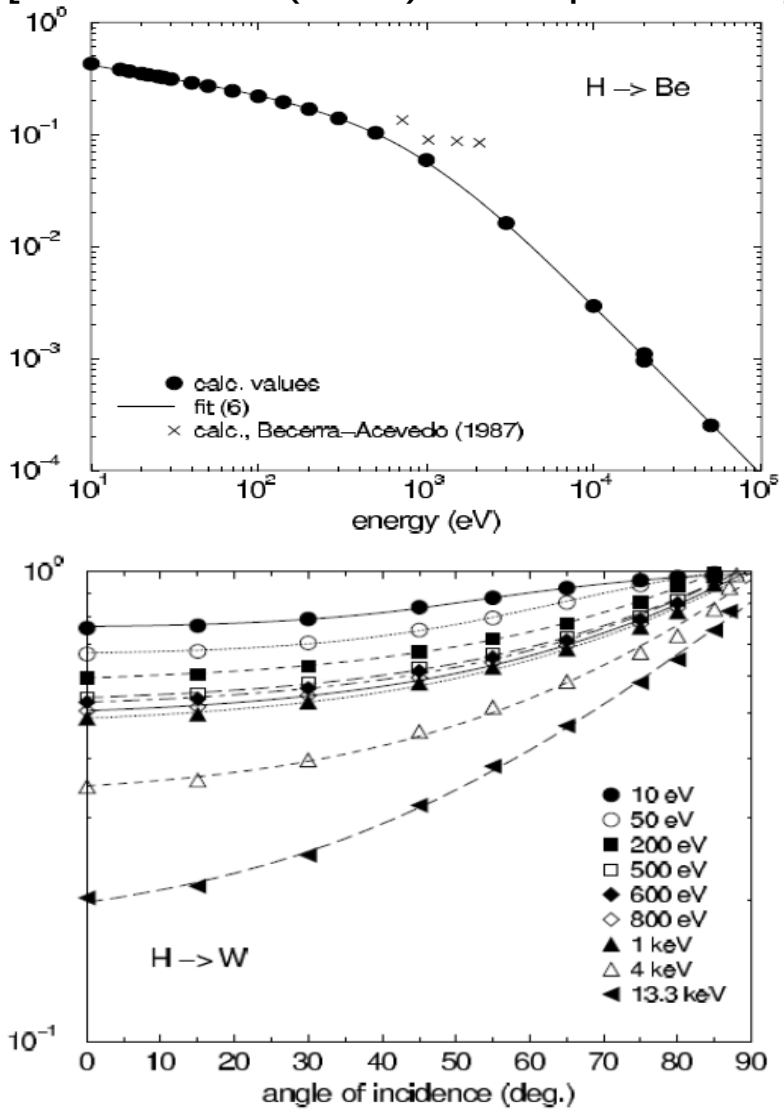

Upper: *H on polycrystalline Be at normal incidence*
Lower *H on polycrystalline W as a function of incident angle*

Small-scale melt dynamics

2D ANSYS Fluent Navier-Stokes simulations

of liquid beryllium flowing over a right-angle corner

- Liquid layer with height h injected at average velocity v
- Variety of flow regimes for tokamak (JET-ILW) relevant conditions

$h = 200\ \mu\text{m}, v = 3\ \text{m/s}$

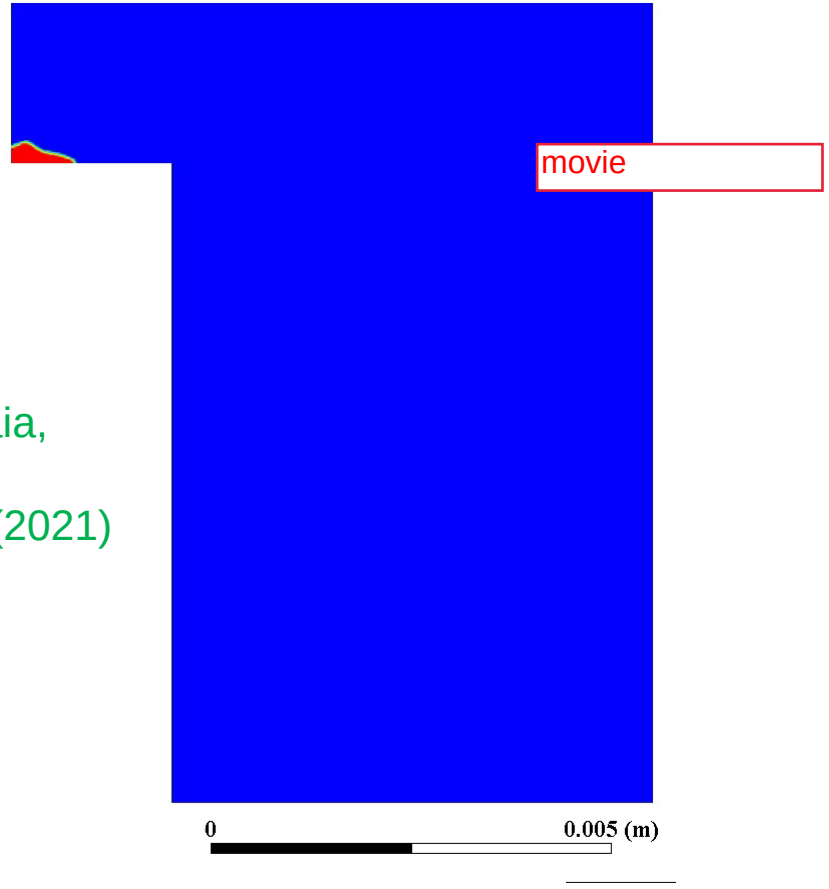

_metal) (Time=2.0033e-04)

$h = 300\ \mu\text{m}, v = 3\ \text{m/s}$

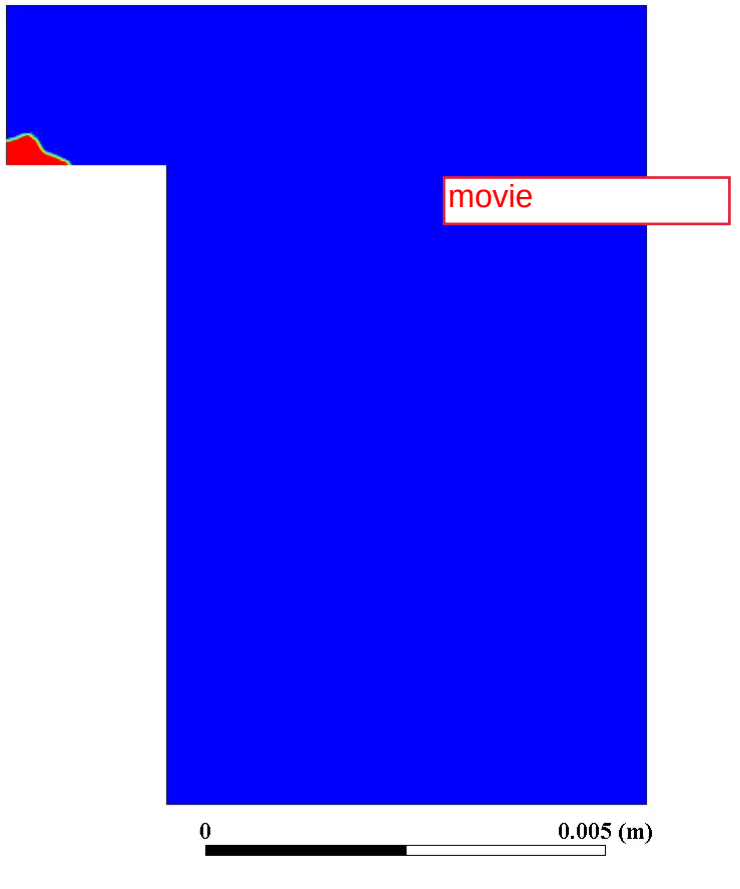

(Time=2.0022e-04)

L. Vignitchouk, S. Ratynskaia, R. Pitts and M. Lehnen, Nuclear Fusion, submitted (2021)

Large-scale melt dynamics

PFC melting: Scale separation and shallow water assumption

- Very large ratio between the melt pool depth and its extension, as revealed by experiments

  K. Krieger *et al., Nucl. Fusion* **58**, 026024 (2018);
  J. W. Coenen *et al.*, *Nucl. Fusion* **55**, 023010 (2015);
  I. Jepu *et al Nucl. Fusion* **59**, 086009 (2019).

- The shallow water approximation → depth-integration of the Navier-Stokes equations → drastic computational cost reduction while retaining sufficient physics for adequate *large-scale* motion description

  C. B. Vreugdenhil *Numerical Methods for Shallow Water Flow* (Dordrecht, Springer, 1994).

- Originally incorporated in the MEMOS-3D code B. Bazylev and H. Wuerz, *J. Nucl. Mater.* **307–311**, 69 (2002)
  Invalid assumption of negligible melt displacement, omission of the bulk replacement current physics and lack of rigorous boundary conditions

- MEMOS-U developed to describe macroscopic melt dynamics in large deformation - long displacement regimes where the melt spills onto a progressively colder solid surface

  S. Ratynskaia, E. Thorén, P. Tolias *et al., Nucl. Fusion* **60**, 104001 (2020).
  E. Thorén, S. Ratynskaia, P. Tolias *et al., Plasma Phys. Control. Fusion* **63**, 035021 (2021).

Macroscopic motion of liquid melts

Governed by the set of incompressible resistive thermoelectric magnetohydrodynamic (TEMHD) equations together with the convection-diffusion equation for the temperature Shercliff J. A. 1979 *J. Fluid Mech.* **91** 231

$$\nabla \cdot \boldsymbol{v} = 0,$$

$$\rho_m \left[\frac{\partial \boldsymbol{v}}{\partial t} + (\boldsymbol{v} \cdot \nabla)\, \boldsymbol{v} \right] = -\nabla p + \mu \nabla^2 \boldsymbol{v} + \boldsymbol{J} \times \boldsymbol{B},$$

$$\rho_m c_p \left[\frac{\partial T}{\partial t} + \boldsymbol{v} \cdot \nabla T \right] = \nabla \cdot (k \nabla T - S T \boldsymbol{J}) + \boldsymbol{J} \cdot \boldsymbol{E},$$

$$\nabla \times \boldsymbol{E} = -\frac{\partial \boldsymbol{B}}{\partial t},$$

$$\nabla \times \boldsymbol{B} = \mu_0 \boldsymbol{J},$$

$$\boldsymbol{J} = \sigma_e \left(\boldsymbol{E} + \boldsymbol{v} \times \boldsymbol{B} - S \nabla T \right),$$

(v, T) fluid velocity, temperature,
$(p, \boldsymbol{J})$ fluid pressure, current density,
$(\boldsymbol{B}, \boldsymbol{E})$ magnetic flux density, electric field strength,
(ρ_m, c_p) mass density, heat capacity
(k, S) thermal conductivity, thermoelectric power,
(μ, γ) dynamic viscosity, surface tension
(σ_e, μ_0) electrical conductivity, vacuum permeability

Macroscopic motion of liquid melts

Governed by the set of incompressible resistive thermoelectric magnetohydrodynamic (TEMHD) equations together with the convection-diffusion equation for the temperature

Shercliff J. A. 1979 *J. Fluid Mech.* **91** 231

Reduction of fluid equations based on:
Shallow water approximation

$$\nabla \cdot \boldsymbol{v} = 0,$$

$$\rho_m \left[\frac{\partial \boldsymbol{v}}{\partial t} + (\boldsymbol{v} \cdot \nabla)\, \boldsymbol{v} \right] = -\nabla p + \mu \nabla^2 \boldsymbol{v} + \boldsymbol{J} \times \boldsymbol{B},$$

$$\rho_m c_p \left[\frac{\partial T}{\partial t} + \boldsymbol{v} \cdot \nabla T \right] = \nabla \cdot (k \nabla T - S T \boldsymbol{J}) + \boldsymbol{J} \cdot \boldsymbol{E},$$

$$\nabla \times \boldsymbol{E} = -\frac{\partial \boldsymbol{B}}{\partial t},$$

$$\nabla \times \boldsymbol{B} = \mu_0 \boldsymbol{J},$$

$$\boldsymbol{J} = \sigma_e \left(\boldsymbol{E} + \boldsymbol{v} \times \boldsymbol{B} - S \nabla T \right),$$

(v, T) fluid velocity, temperature,
$(p, \boldsymbol{J})$ fluid pressure, current density,
$(\boldsymbol{B}, \boldsymbol{E})$ magnetic flux density, electric field strength,
(ρ_m, c_p) mass density, heat capacity
(k, S) thermal conductivity, thermoelectric power,
(μ, γ) dynamic viscosity, surface tension
(σ_e, μ_0) electrical conductivity, vacuum permeability

Macroscopic motion of liquid melts

Governed by the set of incompressible resistive thermoelectric magnetohydrodynamic (TEMHD) equations together with the convection-diffusion equation for the temperature

Shercliff J. A. 1979 *J. Fluid Mech.* **91** 231

$$\nabla \cdot \boldsymbol{v} = 0,$$

Reduction of fluid equations based on:
Shallow water approximation

$$\rho_m \left[\frac{\partial \boldsymbol{v}}{\partial t} + (\boldsymbol{v} \cdot \nabla)\, \boldsymbol{v} \right] = -\nabla p + \mu \nabla^2 \boldsymbol{v} + \boldsymbol{J} \times \boldsymbol{B},$$

$$\rho_m c_p \left[\frac{\partial T}{\partial t} + \boldsymbol{v} \cdot \nabla T \right] = \nabla \cdot (k \nabla T - S T \boldsymbol{J}) + \boldsymbol{J} \cdot \boldsymbol{E},$$

$$\nabla \times \boldsymbol{E} = -\frac{\partial \boldsymbol{B}}{\partial t},$$

$$\nabla \times \boldsymbol{B} = \mu_0 \boldsymbol{J},$$

$$\boldsymbol{J} = \sigma_e \left(\boldsymbol{E} + \boldsymbol{v} \times \boldsymbol{B} - S \nabla T \right),$$

(v, T) fluid velocity, temperature,
$(p, \boldsymbol{J})$ fluid pressure, current density,
$(\boldsymbol{B}, \boldsymbol{E})$ magnetic flux density, electric field strength,
(ρ_m, c_p) mass density, heat capacity
(k, S) thermal conductivity, thermoelectric power,
(μ, γ) dynamic viscosity, surface tension
(σ_e, μ_0) electrical conductivity, vacuum permeability

Simplifications of the field equations based on:

- Magnetostatic limit
- $\boldsymbol{B} = \boldsymbol{B}_{ext}$
- Uniform material composition

MEMOS-U model

$$\frac{\partial h}{\partial t} + \nabla_{\mathrm{t}} \cdot (h\boldsymbol{U}) = \frac{\partial b_1}{\partial t} - \dot{x}_{\mathrm{vap}} \,,$$

$$\rho_{\mathrm{m}} \left[\frac{\partial \boldsymbol{U}}{\partial t} + (\boldsymbol{U} \cdot \nabla_{\mathrm{t}})\, \boldsymbol{U} \right] = \langle (\boldsymbol{J} \times \boldsymbol{B})_{\mathrm{t}} \rangle - \nabla_{\mathrm{t}} P - 3\frac{\mu}{h^2}\boldsymbol{U} + \mu \nabla_{\mathrm{t}}^2 \boldsymbol{U} + \frac{3}{2h}\left(\frac{\partial \gamma}{\partial T} \nabla_{\mathrm{t}} T_{\mathrm{s}} + \boldsymbol{f}_{\mathrm{d}} \right) \,,$$

$$\rho_{\mathrm{m}} c_{\mathrm{p}} \left[\frac{\partial T}{\partial t} + \boldsymbol{U} \cdot \nabla_{\mathrm{t}} T \right] = \nabla \cdot (k \nabla T) + \rho_{\mathrm{e}} |\boldsymbol{J}|^2 - T\frac{\partial S}{\partial T} \boldsymbol{J} \cdot \nabla T \,,$$

$$\nabla \cdot (\sigma_{\mathrm{e}} \nabla \psi) = 0 \quad \text{with } \boldsymbol{J} = -\sigma_{\mathrm{e}} \nabla \psi \,,$$

(U) depth-averaged fluid velocity,
(h, P) melt column height, ambient pressure
$(\boldsymbol{J}, \boldsymbol{B})$ current density, magnetic flux density,
$(b_1, \dot{x}_{vap})$ solidification interface, rate of change of interface position due to vaporization,
(T, T_s) bulk and surface temperature
(ρ_m, c_p) mass density, heat capacity
(k, S) thermal conductivity, thermoelectric power,
(μ, γ) dynamic viscosity, surface tension
(σ_e, μ_0) electrical conductivity, vacuum permeability
(ψ) auxiliary potential

Liquid-solid phase transition: heat integration method
(the enthalpy budget is kept by an extra set of algorithms)

Boundary conditions:

$(k\nabla T - STJ) \cdot \hat{n} = q_{\mathrm{inc}} - q_{\mathrm{cool}}$, q_{inc} is the incident heat flux and and q_{cool} is the surface cooling fluxes

$\sigma_{\mathrm{e}} \frac{\partial \psi}{\partial n} = J_{\mathrm{surf}}$, J_{surf} is the current density on the surface

External input: $q_{inc}, J_{surf}, \boldsymbol{f}_d, \nabla \mathrm{P}_{plasma}$ + geometry and B field

Why the shallow water works well?

Liquid metal on its own solid – excellent wetter

Liquid metals wet their own solid excellently due to the strong interfacial bonding

Eustathopoulos N., Nicholas M.G.,Drevet B. 1999 *Wettability at High Temperatures* (Oxford: Pergamon)

Strong interplay between wetting and resolidification (short ELM duration): Spreading dynamics do not fully evolve, signature capillary waves frozen by resolidification

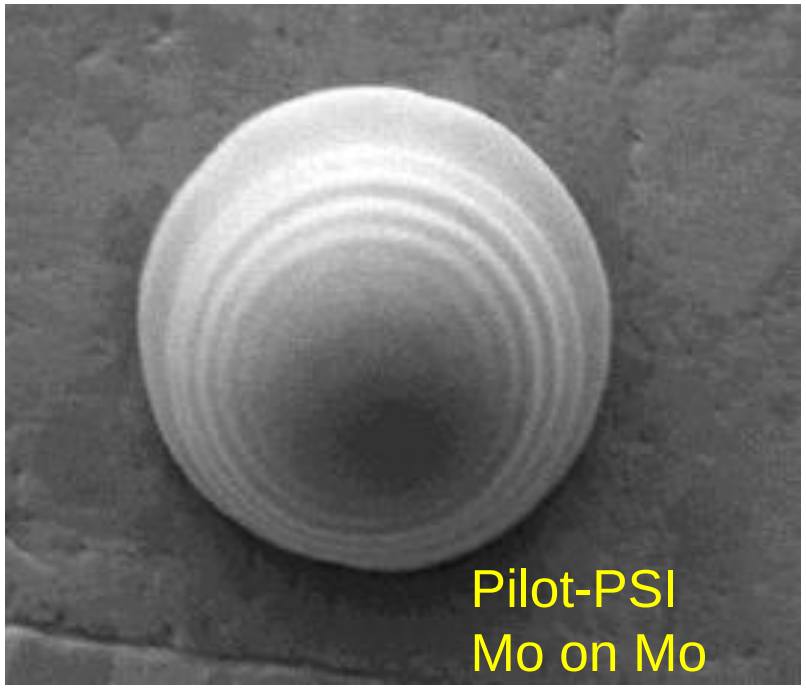

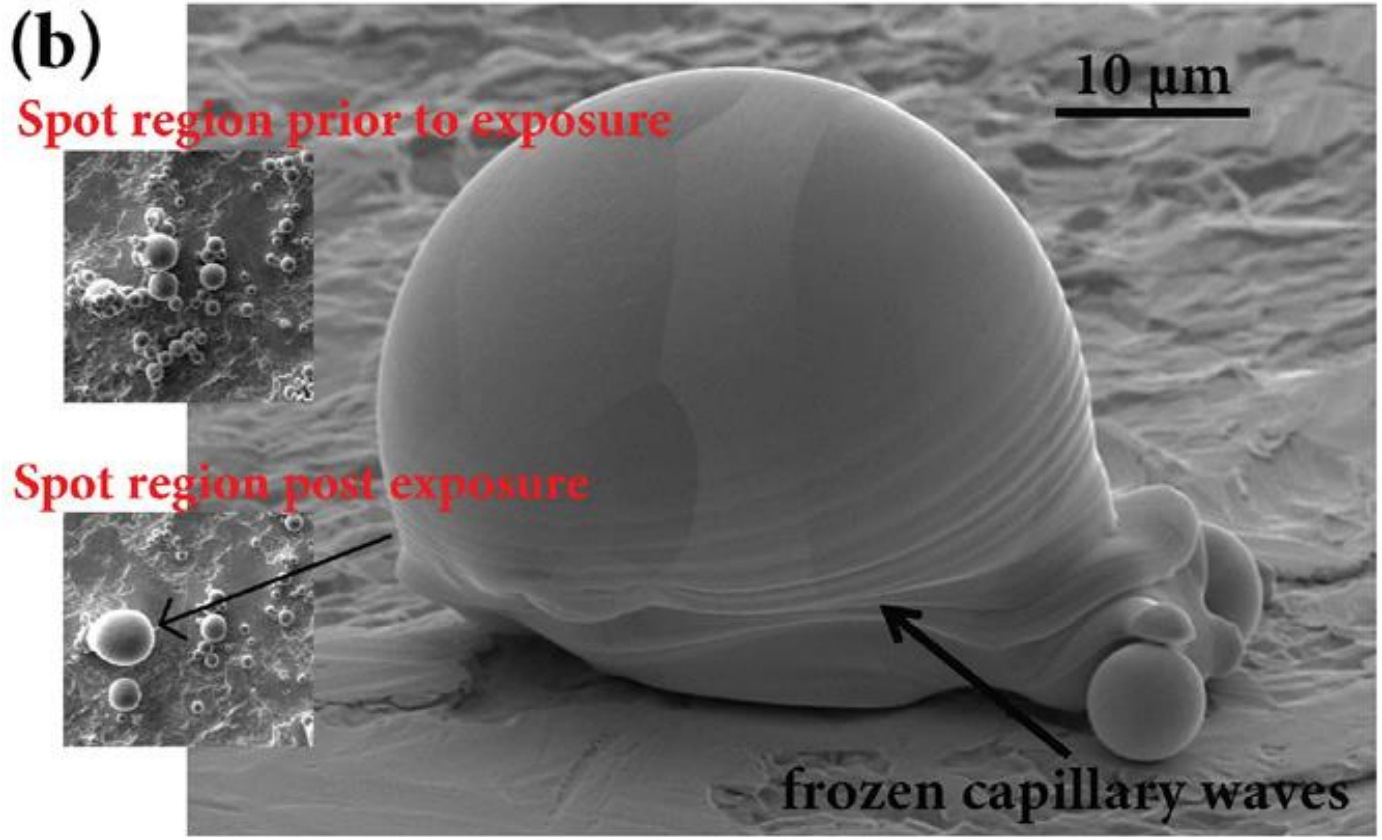

Ratynskaia et al, Nucl. Fusion **56** (2016) 066010

Exercise: liquid W pushed out from a pool by const uniform F

2D Navier-Stokes
customized ANSYS Fluent set-up as in
L. Vignitchouk NME **25** (2020) 100826

Pool size: 0.1 mm x 2 mm
F=45 MN/m^3
equilibrium contact angle 10°

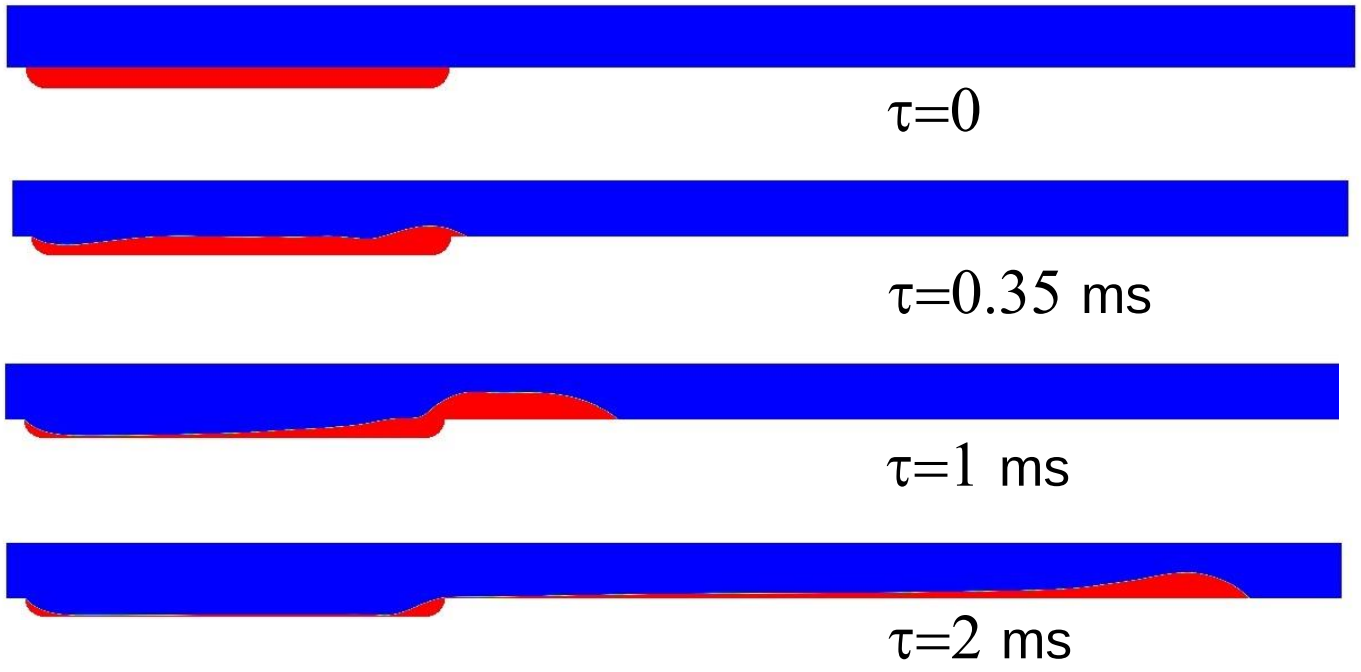

Such dynamics is not captured in shallow water model of MEMOS-U *yet* good agreement with the final deformation profiles observed in multiple experiments is reached

Resolidification-controlled melt dynamics

AUG
W **LE**

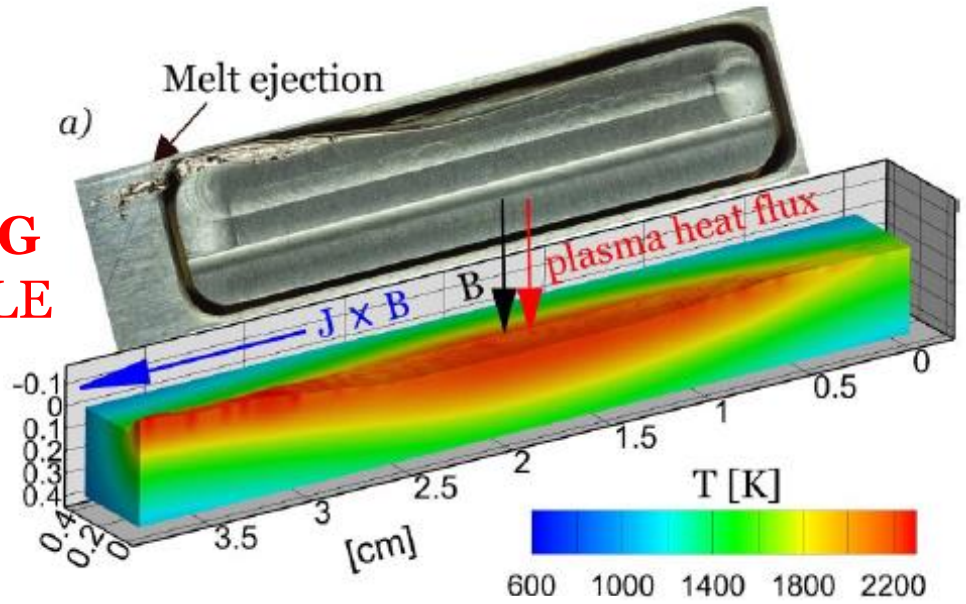

JET
Be **UDP**

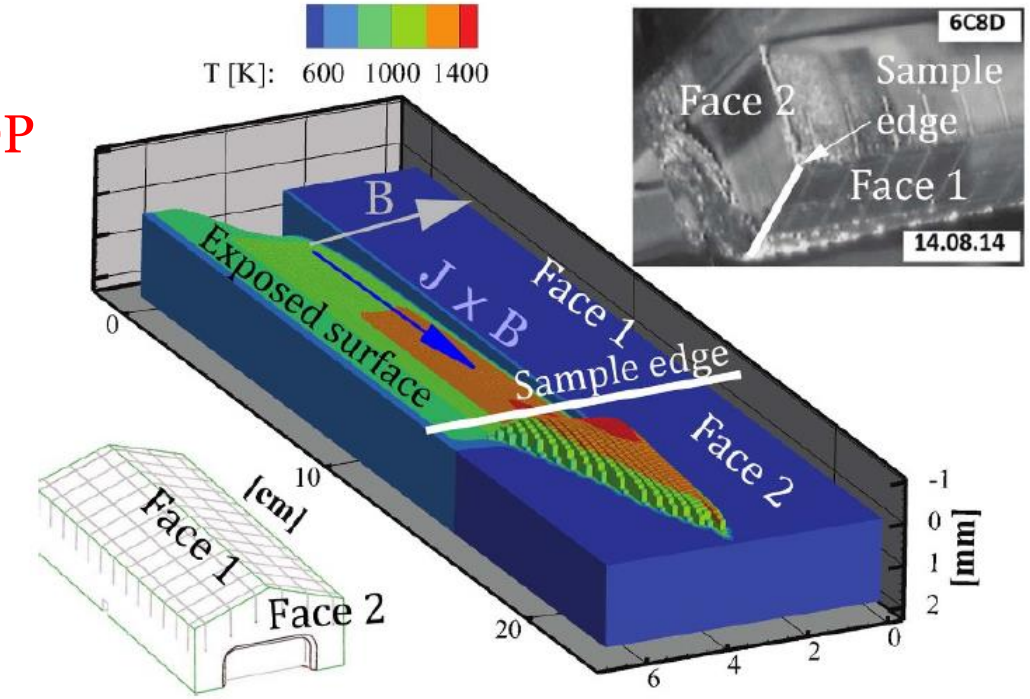

JET
W **LE**

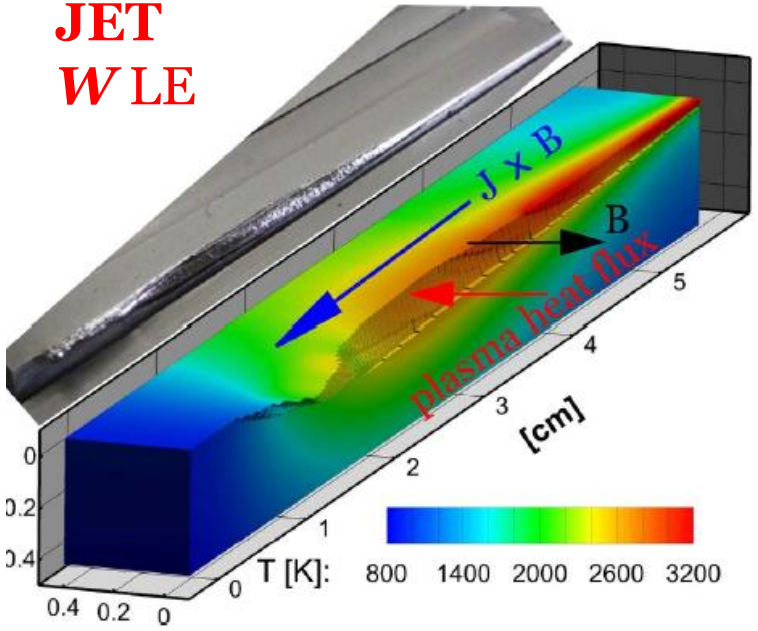

- A unified description of ELM-induced W divertor melting & disruption-induced Be first wall melting
- A quantitative agreement with observations with the only heat flux variations allowed strictly within experimental uncertainties

Ratynskaia, Thoren, Tolias *et al* Nucl. Fusion **60** (2020) 104001

Surface cooling fluxes

MEMOS-U surface terms: *the surface cooling flux*

$$q_{cool} = q_{te} + q_{vap} + q_{rad}$$

- Thermionic cooling $q_{te} = \frac{J_{th}}{e}(W_f + 2\,k_B T_s)$
- Vapor cooling $q_{vap} = \frac{\Gamma_M}{m_a}(h_{vap} + 2\,k_B T_s)$

$$\Gamma_M = P_{vap}\sqrt{\frac{m_a}{2\pi k_B T_s}}$$

P_{vap} scales exponentially with T_s

- Thermal radiation cooling $q_{rad} = \sigma_{SB}\,\varepsilon_T T_s^4$

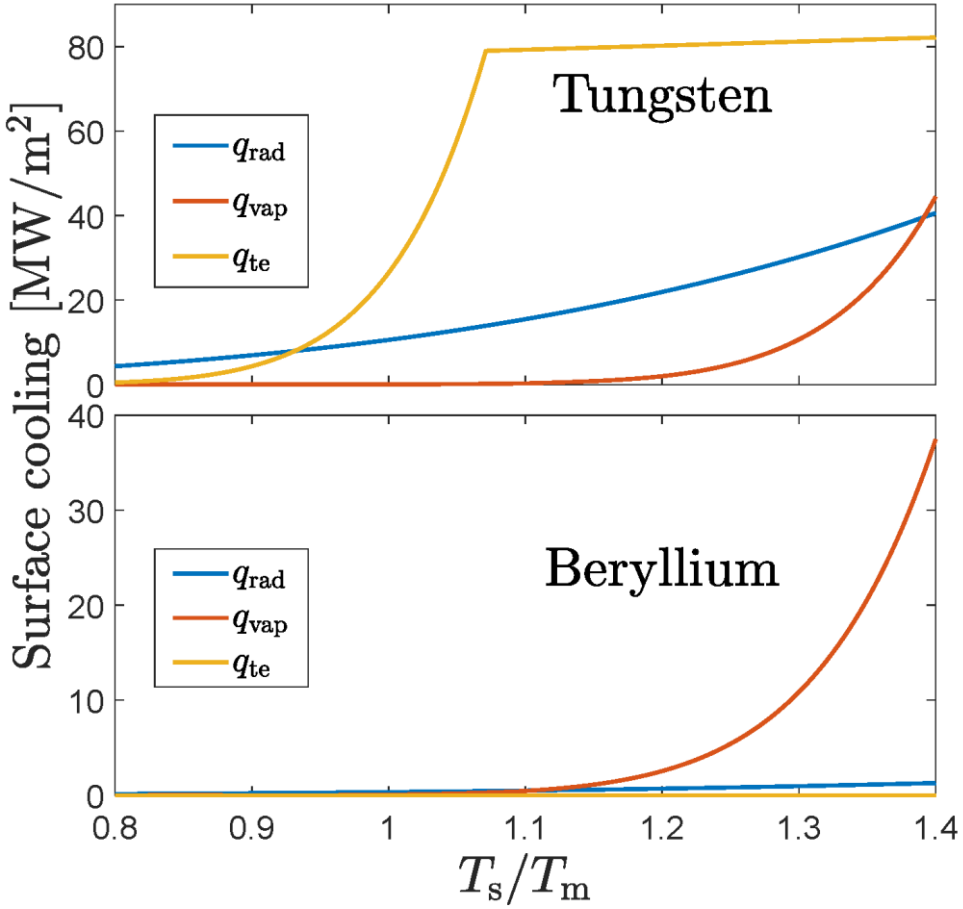

W and Be surface cooling fluxes as a function of the (normalized) surface temperature. TE cooling flux calculated for a representative heat flux q_{inc}=1 GW/m^2.

Main cooling channels: thermionic emission

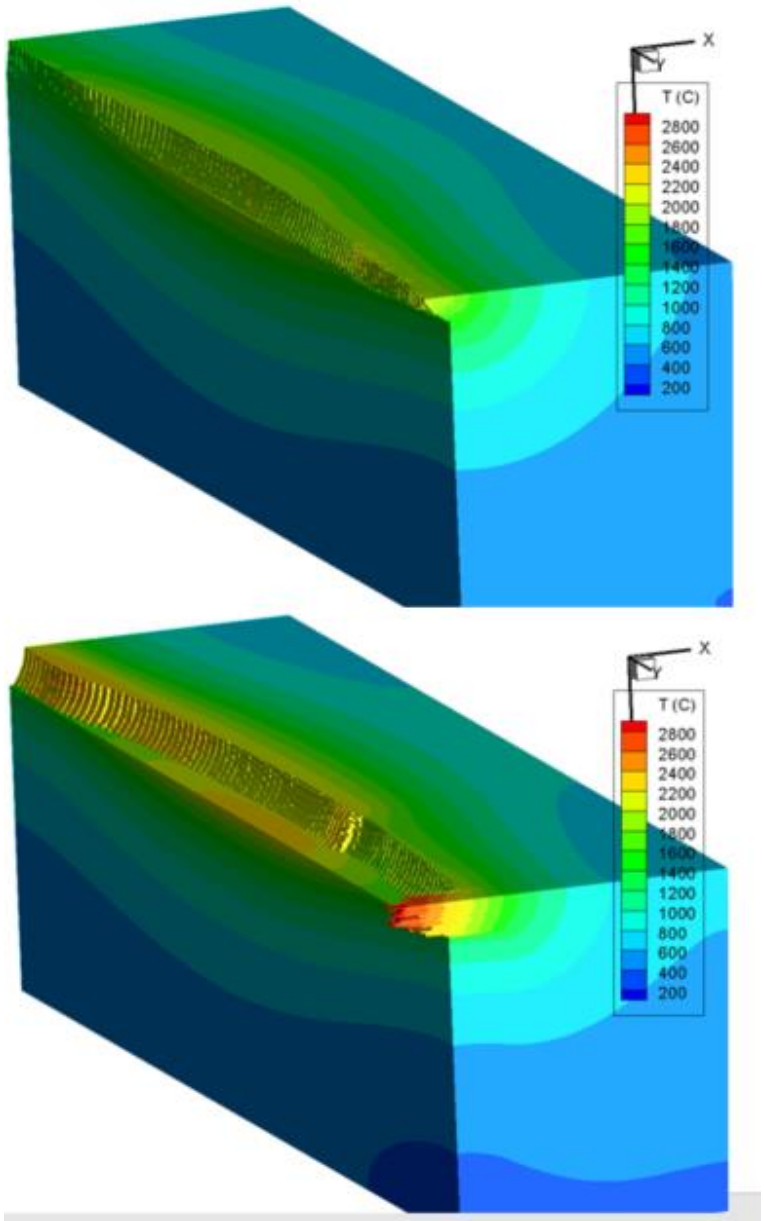

MEMOS-U simulations of the AUG W leading edge melting during pulse #33509

Upper figure: simulations **including thermionic cooling reproduce the surface erosion profile** and total excavated material volume with good accuracy.

Lower figure: simulations **neglecting thermionic cooling lead to ten times higher excavated volume** and much more material ejection from the edge

Ratynskaia, Thorén, Tolias *et al.*, *Phys. Scr.* **96**, 124009 (2021)

Heat load:

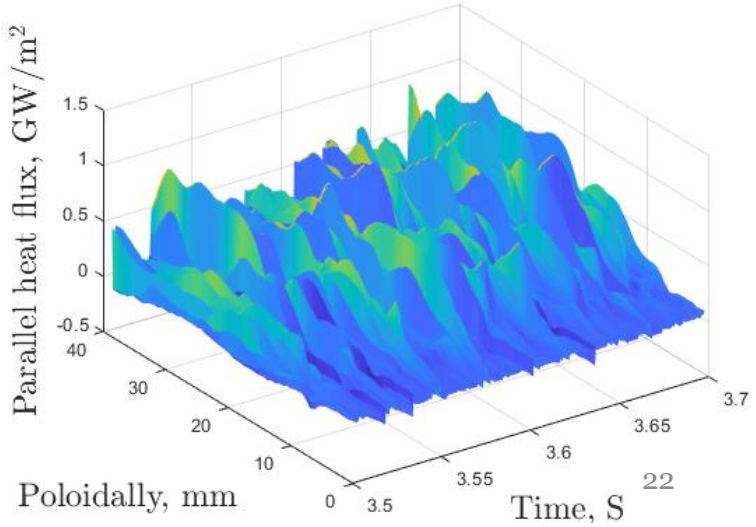

MEMOS-U surface terms: *the current density*

Thermionic emission (**TE**) current:

- Of importance for W only, no role for Be due to low melting point
- The escaping TE triggers a replacement current that flows through the melt layer and generates the dominant **J** x **B** force density.
- It also constitutes a powerful cooling channel
- MEMOS-U escaping TE current density is self-consistently calculated as

$$J_{th} = min\,\{J_{\mathrm{th}}^{\mathrm{nom}}, J_{\mathrm{th}}^{\mathrm{lim}}\}$$

Komm, Ratynskaia, Tolias *et al* 2017 PPCF **59** 094002,
Komm, Tolias, Ratynskaia *et al* 2017 Phys. Scr. 014069
Komm, Ratynskaia, Tolias, Podolnik, 2020, NF Letters, **60** 054002

Halo current:

- Surface current density is an external input

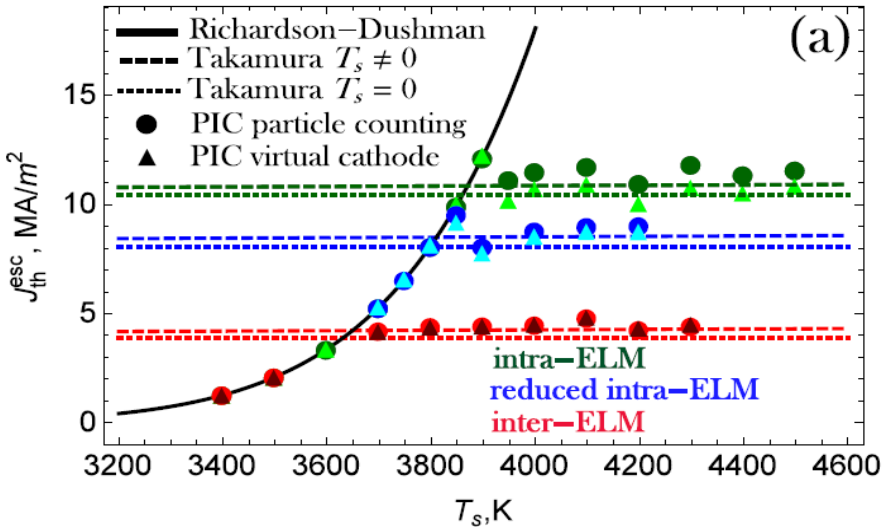

Escaping TE vs surface temperature

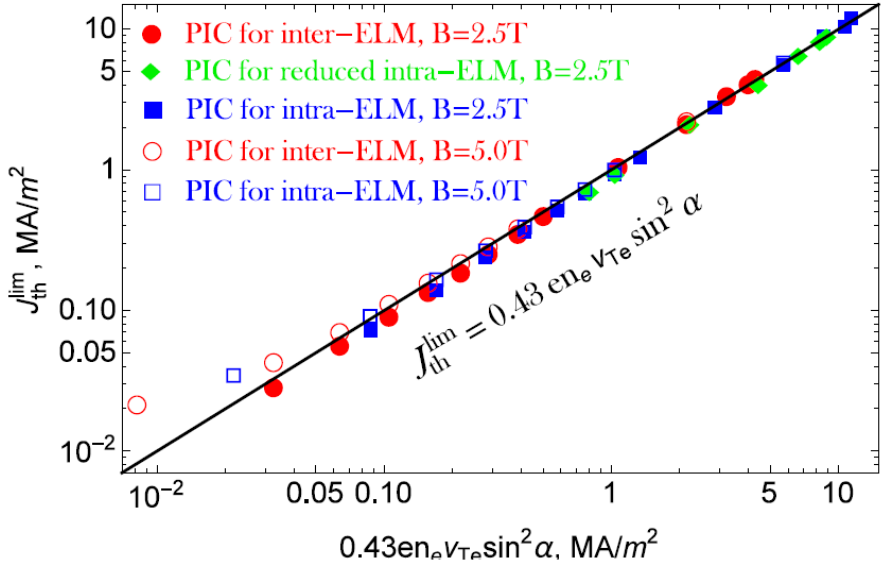

Escaping TE scaling with inclination angle

Modelling of strongly emissive magnetized sheaths

Problem postulation

- Unimpeded thermionic emission from W PFCs at T_s >T_m can drastically, up to orders of magnitude, exceed the incident plasma fluxes.

- Such imbalance cannot be sustained by standard quasi-neutral pre-sheaths and thus modifications of the sheath structure occur to suppress emission.
- Ultimately, only a small percentage of the emitted electron flux is allowed to escape away from the surface (escaping thermionic current density).

- Electron emission can be suppressed by two mechanisms
  - Space charge effects, where a potential well or virtual cathode forms which electrostatically repels a fraction of the emitted electrons back to the surface
  - Prompt re-deposition (only in the presence of inclined magnetic fields), where a fraction of the emitted electrons is recaptured by the surface during their first Larmor gyration

Implementation

- Simulations of biased emitting surface to emulate a grounded surface as the majority of tokamak conducting PFCs are electrically connected to the grounded vessel.

- Simplifying assumption that the locally emitting surface of limited area does not alter the global plasma potential ($\sim -3T_e$) given the vast area of the grounded vessel wall.

- The situation can certainly be more complicated, but for *a restricted emitting surface*, this assumption is still more relevant than that of a fully floating PFC whose potential, depending on the strength of emission, can assume arbitrary values including those above the plasma potential (the inverse sheath) [Campanell & Umansky, PRL **116** (2016) 085003; Campanell & Johnson, PRL **122** (2019) 015003, Campanell PoP **27**, 042511 (2020)].

- In our simulations, the balance between the plasma electron fluxes and the ion fluxes is maintained. Consequently, a finite current is flowing through the PFC (in order to compensate for the loss of bound electrons) that is equal to the *escaping* thermionic current.

- This is fully consistent with the picture of the replacement current that leads to the $\vec{\boldsymbol{J}} \times \vec{\boldsymbol{B}}$ force density which drives macroscopic melt motion

SCL regime for magnetized sheaths

- In un-magnetized plasmas, non-monotonic SCL sheath potential profiles lead to escaping current densities J_{esc} that remain approximately constant as the strength of emission increases for given plasma conditions
- In the case of dominant thermionic emission, this implies that J_{th}^{esc} as a function of the surface temperature T_s follows the unimpeded Richardson-Dushman curve up to a plasma-dependent plateau, beyond which it becomes T_s-independent

[M. Komm, P. Tolias, S. Ratynskaia *et al.*, Phys. Scr. **T170** (2017) 014069]

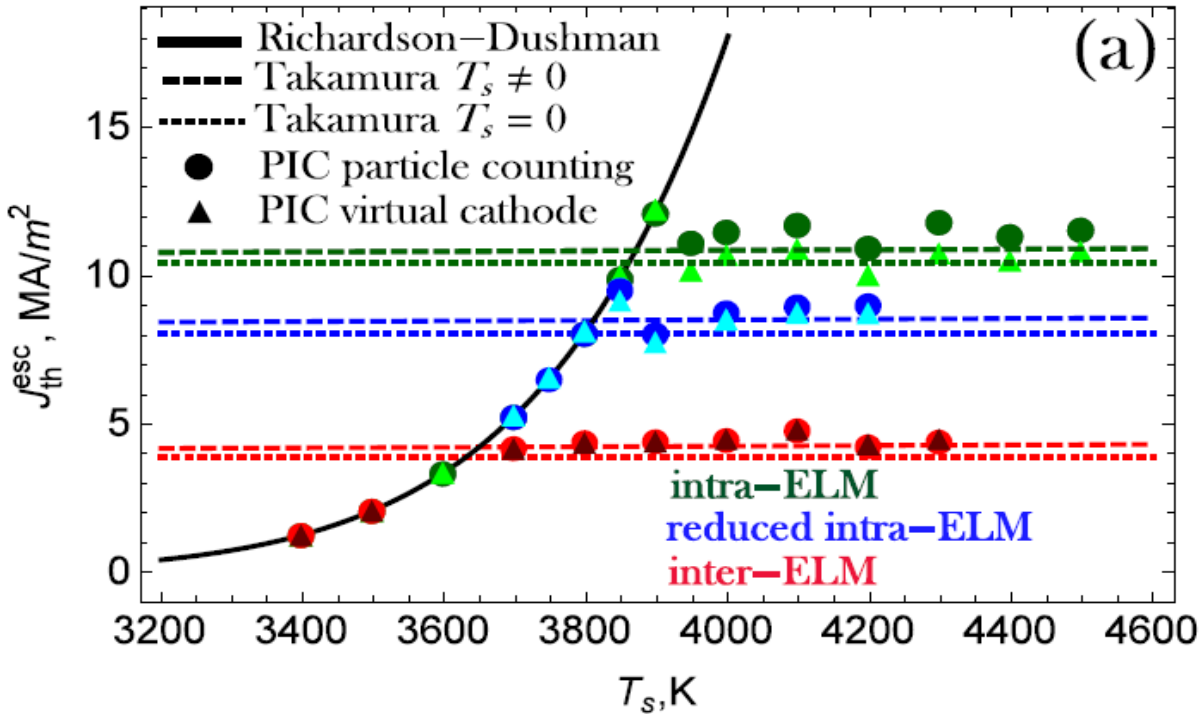

In magnetized plasmas, due to the two-dimensional nature of the problem as well as prompt re-deposition, such strict limitation of the escaping thermionic current J_{th}^{esc} cannot be taken for granted.

Semi-empirical formula for $J_{\mathrm{th}}^{\mathrm{lim}}$

- The semi-empirical expression, $J_{\mathrm{th}}^{\mathrm{lim}}(n_{\mathrm{e}}, T_{\mathrm{e}}, B, \alpha) \simeq J_{\mathrm{th}}^{\mathrm{lim}}(n_{\mathrm{e}}, T_{\mathrm{e}}, 90^{\mathrm{o}})\sin^2\alpha$, revealed by extensive PIC simulations, was interpreted on the basis of the Chodura picture of inclined magnetized sheaths and a single particle field-free approximation of prompt re-deposition.

- The Child-Langmuir expression that completes the scaling law, $J_{\mathrm{th}}^{\mathrm{lim}}(n_{\mathrm{e}}, T_{\mathrm{e}}, 90^{\mathrm{o}}) \simeq 0.43 e n_e v_{Te}$, also revealed by PIC simulations, was reproduced from the Takamura system of equations.

S. Takamura et al, Contrib. Plasma Phys. 44 (2004)

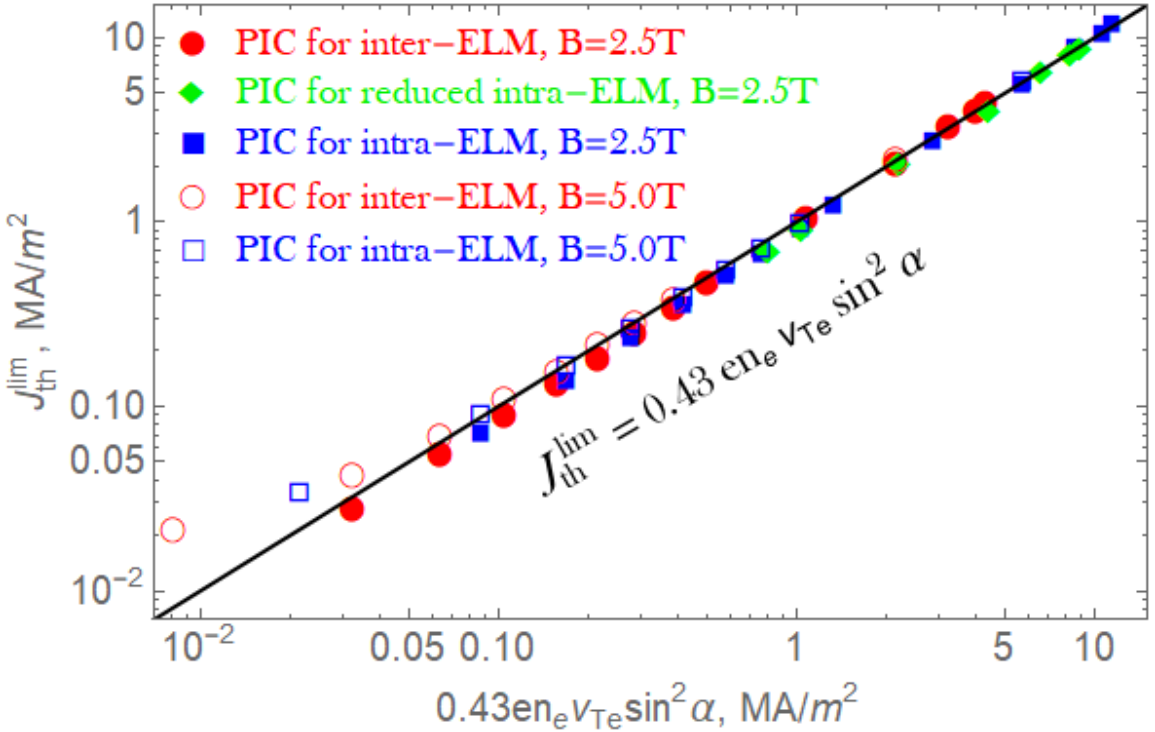

The relative errors are less than 20% regardless of the plasma parameters / B-field provided that $\alpha > 5^{\mathrm{o}}$

Komm, Ratynskaia, Tolias, Podolnik, 2020, NF Letters, **60** 054002

Summary

- Vast scale separation of PFC melt events forbids brute force calculations.

- Ideally plasma should be a ghost (not real) fluid, whose effects are imposed through the boundary conditions on the free surface → often beyond the customization capabilities of commercial software

- Large scale treatment can rely on shallow water assumptions which is
  - adequate for characteristic dimensions of melt pools induced by high transient loads on PFCs
  - works well due to prominent role of the re-solidification in the melt dynamics

- MEMOS-U describes macroscopic melt dynamics in large deformation - long displacement regimes

- The MEMOS-U code is based on a transparent physics model and is void of adjustable coefficients. The simulation outcome **depends solely on the input of** (i) the incident heat flux, (ii) local magnetic field, (iii) problem geometry for ELM-driven melting, (iv) the halo current density for disruption-driven melting

- MEMOS-U was successfully validated against dedicated EUROfusion experiments including specially designed to test thermionic emission modelling (floating sample connection with the vessel with unusual energy deposition and comparison of poor and good thermionic emitters (Niobium and Iridium),both AUG)

- Agreement with diverse experiments testifies that framework (PIC simulations of biased sample emulating grounded components with restricted emitting area) employed for predictions of limited escaping thermionic current and proposed scaling with B field angle and incoming plasma flux are adequate

OUTLOOK

- The MEMOS-U boundary conditions have been obtained and tested for the parameter space of contemporary tokamaks.

- Even though thermionic emission should remain dominant for W, the emissive sheaths of ITER and DEMO will be much more complicated than those of present-day tokamaks

  P. Tolias, M. Komm, S. Ratynskaia and A. Podolnik, *Nucl. Mater. Energy* **25**, 100818 (2020)

  new systematic PIC studies of the sheath and magnetic pre-sheath are required

- Development of tools with flexibility for imposing general boundary conditions on the free-surface in desired geometry – to allow detailed study of small scale dynamics and metal splashing

- Used in combination with MEMOS-U: large scale predictions to provide basic properties of the pools (depth, speeds, whether the PFC edge can be reached etc) aiming at a self-consistent treatment of the multi-scale problem of PFC melt events

Extra slides

Dynamic boundary conditions on free surface

Only Cauchy stress tensor, the Maxwell stress tensor has a negligible effect under conditions of interest here

Stress balance normal to the surface

$$p\,|_{b_2} - P = \gamma\,\kappa$$

γ the surface tension

κ the free surface curvature

Stress balance tangential to the surface

$$-\mu\,\frac{\partial \boldsymbol{v}_t}{\partial n}\,|_{b_2} = \boldsymbol{f}_d + \nabla_t \gamma$$

$\boldsymbol{f}_d$ the external drag force

for uniform material composition $\nabla_t \gamma$ becomes $\frac{\partial \gamma}{\partial T}\nabla_t T_s$ (thermo-capillary convection)

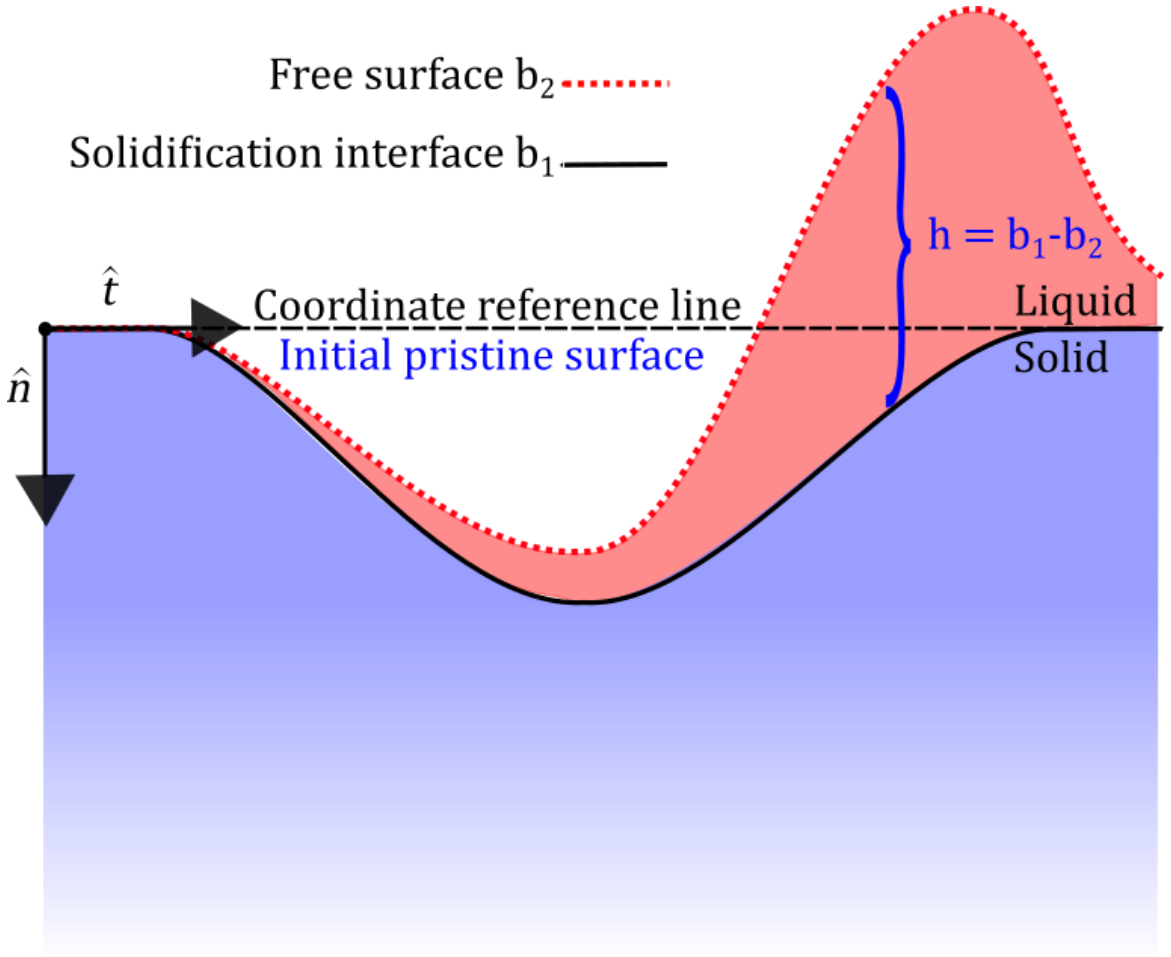

Replacement current

Leading edge sample

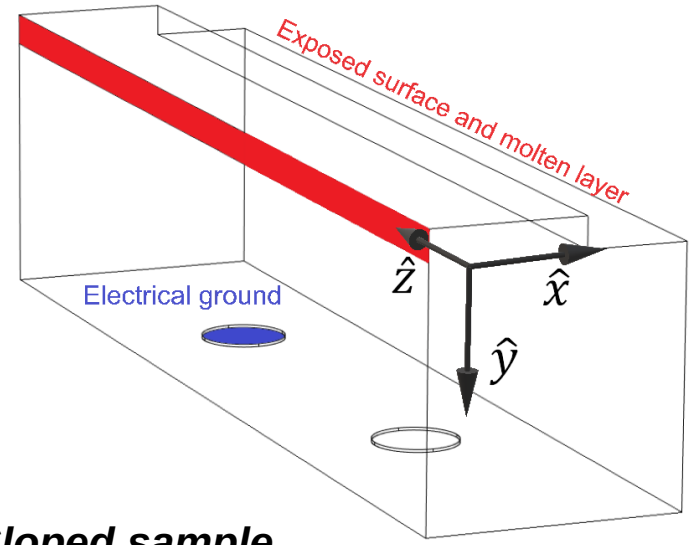

Sloped sample

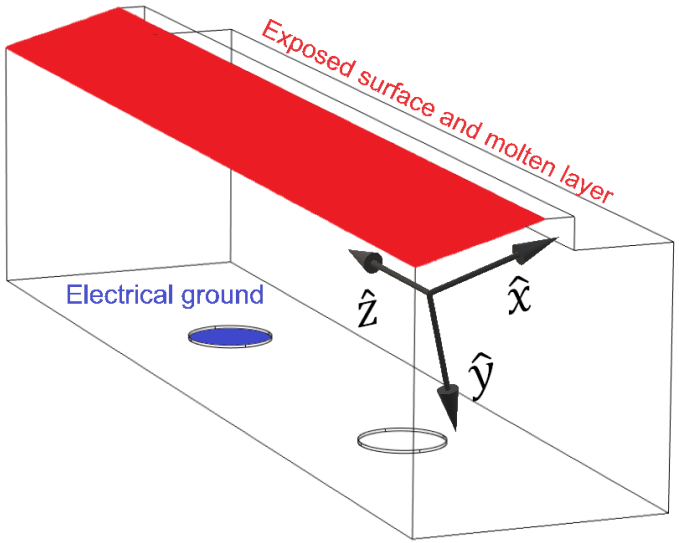

Melt motion by volumetric $\boldsymbol{J} \times \boldsymbol{B}$ force

- $\boldsymbol{B}$ is the toroidal magnetic field
- $\boldsymbol{J}$ is a current density in the liquid metal triggered by escaped thermionic emission emission

$$< J_y >_{\parallel} \backsimeq J_{th}/4$$

Thorén, Tolias, Ratynskaia *et al* NF **58** 2018

Leading edge sample

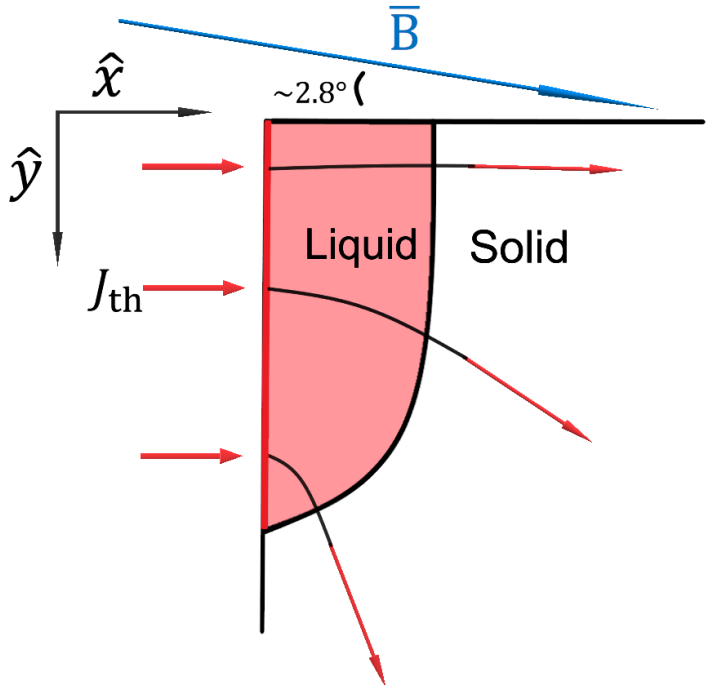

Sloped sample

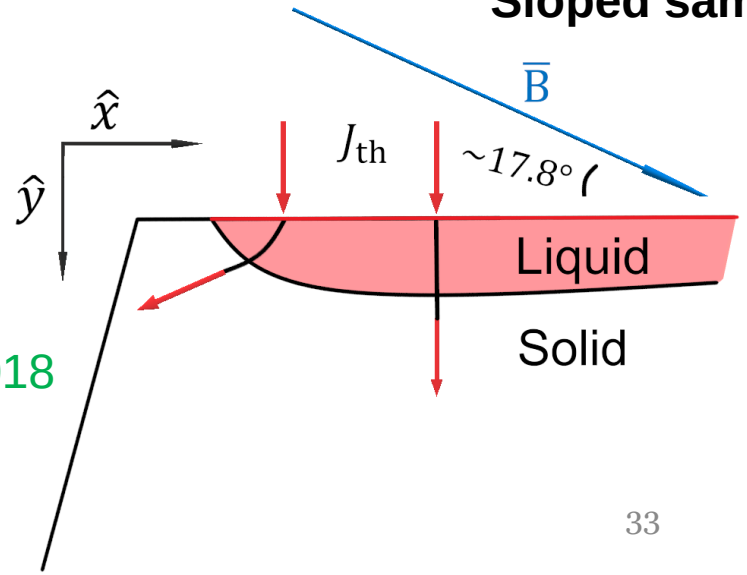

Main acceleration mechanisms

$$\rho\left(\frac{\partial u}{\partial t}+u\frac{\partial u}{\partial x}\right)=-\frac{\partial p}{\partial x}+\boldsymbol{JB}+\mu\frac{\partial^2 u}{\partial x^2}+\frac{3}{2h}\frac{\partial \gamma}{\partial T}\frac{\partial T_s}{\partial x}-\boldsymbol{3\mu\frac{u}{h^2}}+\frac{3}{2}\frac{f_{drag}}{h}$$

ρ is the mass density
u is the depth-averaged velocity
J is the current density
B is the magnetic flux density
μ is the dynamic viscosity
h is the melt layer thickness
γ is the surface tension

- **Main acceleration mechanisms** are Lorenz force JB and viscous depth-shear $3\mu\frac{u}{h^2}$
- $\boldsymbol{h}$ **is always changing**, melt velocity is given by transient balance of acceleration and deceleration

Vapour pressure

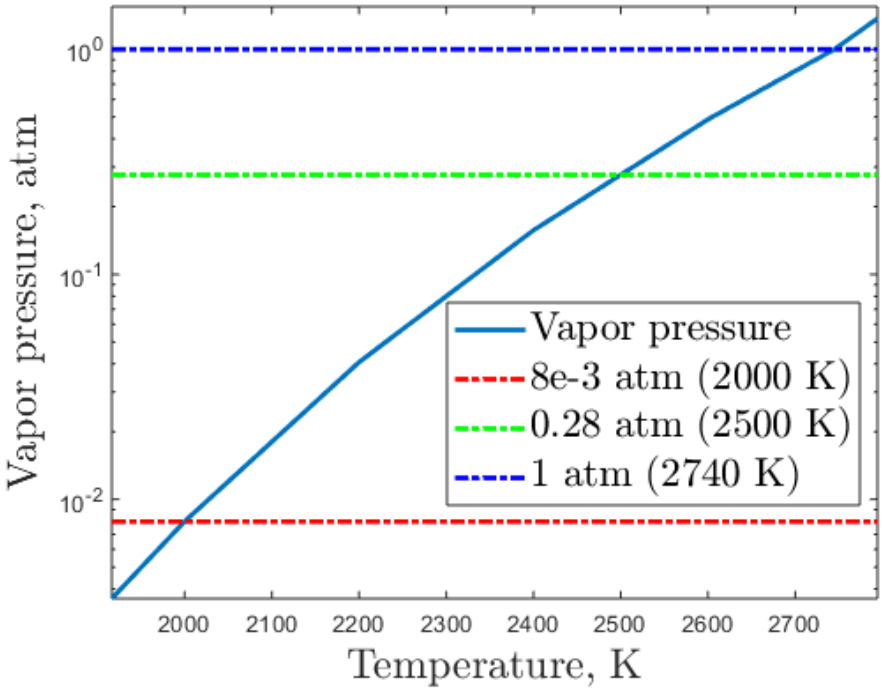

Main cooling channels: convection

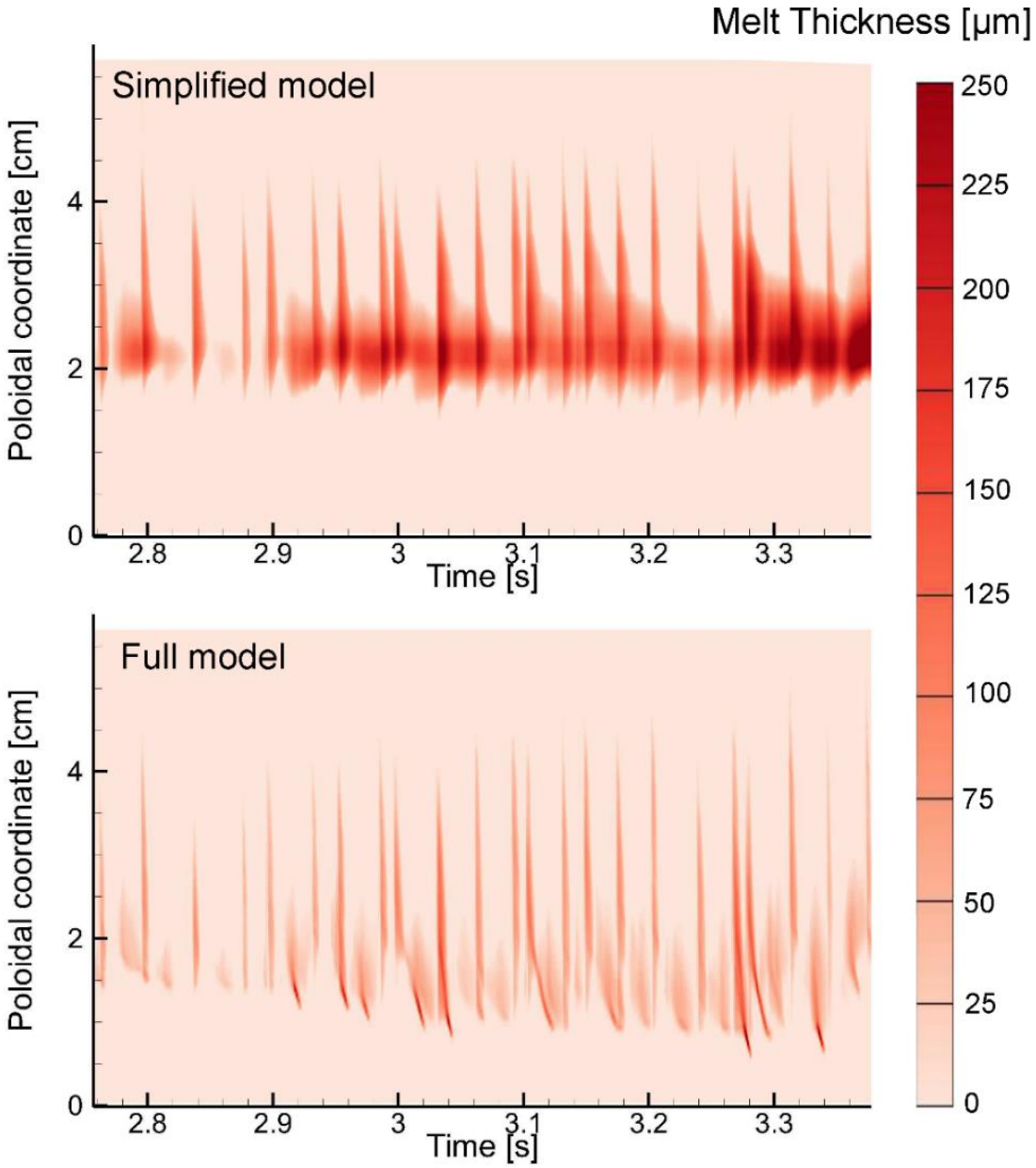

MEMOS-U simulations of the JET W leading edge melting during pulse #84779

Thorén, Ratynskaia, Tolias *et al., PPCF* **63**, 035021 (2021)

The melt layer thickness as function of the exposure time and the poloidal coordinate, for the uppermost part of the sample corner (where the deepest melting occurs) near the end of the exposure. Results for

the upper figure - no convection

the lower figure - the full model

Heat load:

- The typical ELM duration < 3 ms, the average frequency 30 Hz.
- The max ELM heat flux 0.5 -1.5 GW/m^2 and the inter-ELM heat flux 50-200 MW/m^2

PIC studies of TE: Implementation

- During ELMs, the strong spatiotemporal heat flux variations will result to equally strong T_s variations and to surface deformation (due to melt motion). Hence, *each surface element will be characterized by a different surface temperature (T_s), incident heat flux (n_e,T_e) and magnetic field inclination angle with respect to the surface normal (α).*

- The only way to treat such a formidable problem is to assume that the escaping thermionic current contributions from each surface element are independent → PIC simulations with periodic boundary conditions for homogeneous plasmas and with constant T_s can be employed

2D3V PIC code SPICE has been employed

- ✓ The simulated area contains an infinite wall near the lower boundary with a homogeneous prescribed temperature, which is emitting thermionic electrons according to the Richardson-Dushman law $J_{th}^{RD} = A_{eff} T_s^2 \exp(-W_f/k_b T_s)$ with $A_{eff} = 60 \mathrm{Acm^{-2}K^{-2}}$, $W_f = 4.55\mathrm{eV}$ for tungsten.
- ✓ The potential of the wall is fixed at -$3k_b T_e$ with respect to the plasma potential.
- ✓ The ions are injected in the simulation region with a distribution of parallel-to-the-magnetic-field velocities that satisfies the Bohm criterion. The perpendicular component of the ion velocities and all three components of the plasma electron velocities are Maxwellian.
- ✓ The thermionic electrons are injected with a Maxwellian distribution of temperature T_s (half-Maxwellian along the wall normal, full-Maxwellian along the wall tangent plane).
- ✓ Plasma particle injection through the upper boundary is set-up in the cold wall approximation. Possible charge imbalance due to escaping thermionic electrons is self-consistently handled by the potential profile which can prevent part of the plasma particles from entering the domain.